

Interplay and Competition Between Two Different Types of Redox-Active Ligands in Cobalt Complexes: How to Allocate the Electrons?

Lukas Lohmeyer⁺,^[a] Marco Werr⁺,^[a] Elisabeth Kaifer,^[a] and Hans-Jörg Himmel^{*[a]}

Abstract: The field of molecular transition metal complexes with redox-active ligands is dominated by compounds with one or two units of the same redox-active ligand; complexes in which different redox-active ligands are bound to the same metal are uncommon. This work reports the first molecular coordination compounds in which redox-active bisguanidine or urea azine (biguanidine) ligands as well as oxolene ligands are bound to the same cobalt atom. The combination of two

different redox-active ligands leads to mono- as well as unprecedented dinuclear cobalt complexes, being multiple (four or six) center redox systems with intriguing electronic structures, all exhibiting radical ligands. By changing the redox potential of the ligands through derivatisation, the electronic structure of the complexes could be altered in a rational way.

Introduction

Coordination compounds with redox-active ligands are of increasing interest for catalysis and materials science.^[1–10] Especially, cobalt complexes with redox-active ligands were intensively studied in the last decades.^[11–20] Intramolecular electron transfer (IET) between the metal and the redox-active ligand in these complexes is often accompanied by massive changes in the magnetic and optical properties, for example for conversion from a *high-spin* Co^{II} complex with three unpaired electrons to a *low-spin* Co^{III} complex without unpaired electrons.^[11,13–21] Valence tautomerism, denoting a reversible interconversion (originally an equilibrium) between redox isomers, was first discovered for octahedral cobalt complexes with two oxolene ligands.^[22] It was since shown that conversion of one redox isomer into another could be achieved by temperature, both in solution and in the solid state, by light (at low temperature)^[23–29] and by pressure.^[30] The differences in the molecular dipole moments between the two redox isomers could be used to design materials with switchable macroscopic polarization,^[31] inducing electronic pyroelectricity.^[32] Moreover, chemical reactions could induce IET processes. Redox-induced intramolecular electron transfer (RIET), leading to metal reduc-

tion upon overall oxidation of the complex or metal oxidation upon overall reduction, was first experimentally verified for dinuclear cobalt complexes with a bridging redox-active tetraoxolene ligand.^[17,33] Recently, we reported on a RIET process in a mononuclear cobalt complex triggered by hydrogen-bond strengthening.^[34] Moreover, we showed that valence isomerism of octahedrally coordinated cobalt complexes with a redox-active bisguanidine ligand could be initiated by change of the solvent.^[35]

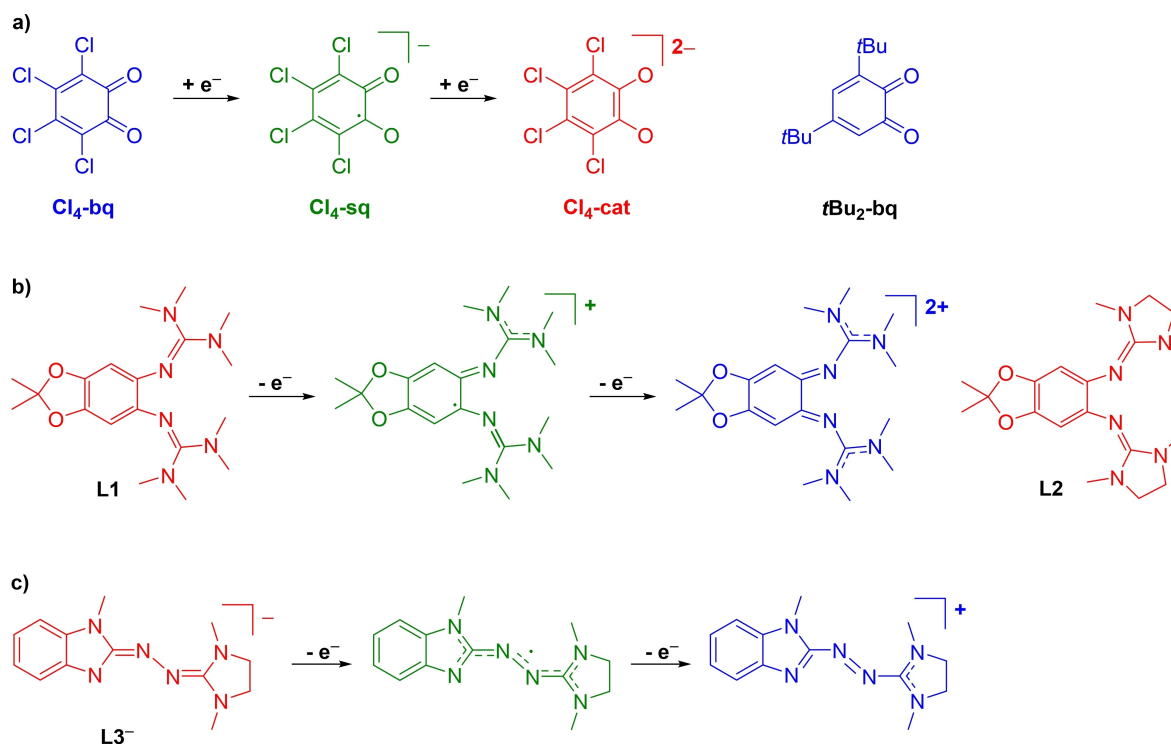
Generally, these complexes exhibit one or more units of the same redox-active ligand. Obviously, the integration of different types of redox-active ligands in the same complex opens up new opportunities for the design of multiple center redox systems and therefore is of great importance for the further development of this field. However, synthetic protocols to obtain such complexes in a rational way are by enlarge missing. Rare examples for complexes with two different ligand-centered redox sites include octahedral Pd or Pt complexes with terminal bis(arylimino)-acenaphthene (BIAN) ligands and 1,3,5-tris(pyridyl)triazine (tpt) linkers,^[36] metal nitrosyls (e.g. ruthenium or iron complexes with a redox-active porphyrin co-ligand^[37,38] or ruthenium complexes with imino-*o*-benzoquinone co-ligands^[39]), and a dinuclear ruthenium complex with two terminal imino-*o*-benzoquinonato ligands and a bridging 2,3,5,6-tetrakis(2-pyridyl)pyrazine π -acceptor bridge.^[40] It should also be mentioned in this context that variations in the π -acceptor character of 2,2'-bipyridine co-ligands could be used to alter the valence-tautomeric conversion in cobalt complexes with two oxolene ligands, but here the 2,2'-bipyridine co-ligands do not change their redox state.^[41] An obstacle for the integration of different types of redox-active ligands is the similar charge regime of the predominantly applied oxolene ligands and related ligands derived from imino-phenols or bisimines, that all are neutral in their oxidised redox states and (formally) anionic in their reduced redox states (see Scheme 1a for the example of tetrachloro-benzoquinone and the corre-

[a] L. Lohmeyer,⁺ M. Werr,⁺ Dr. E. Kaifer, Prof. H.-J. Himmel
Anorganisch-Chemisches Institut
Ruprecht-Karls-Universität Heidelberg
Im Neuenheimer Feld 270, 69120 Heidelberg (Germany)
E-mail: hans-jorg.himmel@aci.uni-heidelberg.de

[⁺] These authors contributed equally to the work.

Supporting information for this article is available on the WWW under <https://doi.org/10.1002/chem.202201789>

© 2022 The Authors. Chemistry - A European Journal published by Wiley-VCH GmbH. This is an open access article under the terms of the Creative Commons Attribution Non-Commercial License, which permits use, distribution and reproduction in any medium, provided the original work is properly cited and is not used for commercial purposes.



Scheme 1. Lewis structures of a) the two *o*-benzoquinones Cl₄-bq and tBu₂-bq, b) the two bisguanidines L1 and L2, and c) the unsymmetric, anionic urea azine L3⁻ used in this work. The Lewis structures of the accessible redox states are also sketched, highlighting the different charge regimes of the ligand types. Colour code used throughout this work: reduced state in red, intermediate in green, oxidised in blue.

spending semiquinone and catecholates formed upon its reduction).

In this work, we report the rational synthesis of new cobalt complexes with two different types of redox-active ligands. We applied one of the neutral redox-active bisguanidines L1 and L2,^[42,43] or monoanionic urea azine L3⁻, in situ generated from the protonated urea azine (biguanidine) precursor HL3,^[44] as one ligand unit (see Lewis structures in Scheme 1). All three ligands are redox-active guanidine-type ligands. They differ in their coordination mode, but all are strong σ - and π -donor ligands in their reduced form. Oxolenes, being well-established ligand systems, serve as second type of redox-active ligand, being either derived from tetrachloro-1,2-benzoquinone (Cl₄-bq) or 3,5-di-tertbutyl-1,2-benzoquinone (tBu₂-bq). In the past, we synthesised cobalt as well as copper complexes using L1 and L2,^[34,36,37,45] and also L3⁻,^[38] but no other redox-active ligand was present in these complexes. Since the bisguanidines/urea azine adopt different redox states in these complexes, they provide suitable reference data for the ligand redox states in the new complexes presented in this work.

All ligands possess three accessible redox states, being illustrated in Scheme 1. In the following, red colour is used for the reduced, electron-rich forms, being neutral (L1 and L2), anionic (L3⁻) or dianionic (Cl₄-cat and tBu₄-cat). On the other hand, blue colour is used for the fully oxidised, electron-poor forms, that are either dicationic (L1²⁺ and L2²⁺), monocationic (L3⁺) or neutral (Cl₄-bq and tBu₄-bq). Then, for each ligand there is an intermediate, radical redox state, marked by green colour.

Most importantly, the charges of the redox states for the two types of redox-active ligands differ. The bisguanidines L1 and L2 are neutral in their reduced redox states, the urea azine is monoanionic in its reduced form (L3⁻), and the oxolene ligands are dianionic in their reduced redox states (Cl₄-cat and tBu₄-cat). It will be shown that the different charge regimes allow the facile synthesis of complexes with both types of ligands.

In a complex, the oxolene-type ligands compete with the bisguanidine/urea azine ligands for the electron density, leading to intriguing electronic properties that are difficult to predict. From cyclic voltammetry measurements, redox potentials ($E_{1/2}$ value) for the benzoquinone/semiquinone couples of -0.33 V for (Cl₄-bq)/(Cl₄-sq) in CH₂Cl₂^[46] (-0.29 V^[47] or -0.27 V^[48] in CH₃CN) and -0.92 V in CH₃CN for (tBu₂-bq)/(tBu₂-sq)^[41] (-0.96 V according to an earlier analysis^[42]) were obtained. For the redox couple (Cl₄-sq)/(Cl₄-cat), $E_{1/2}$ values of -1.19 V in CH₂Cl₂^[40] and -1.06 V^[42] in CH₃CN were reported, and for the redox couple (tBu₂-sq)/(tBu₂-cat), an $E_{1/2}$ value of -1.7 V^[49] was given. Furthermore, for the bisguanidines in CH₂Cl₂ solution, $E_{1/2}$ values of -0.25 V for L1^{•+}/L1,^[36] and -0.46 V for L2^{•+}/L2^[36] were found. Then, $E_{1/2}$ values in CH₂Cl₂ of -0.11 V for L1²⁺/L1^{•+} and -0.38 V for L2²⁺/L2^{•+} were reported. Finally, for the protonated azine ligand, HL3, a redox potential of $E_{1/2} = -0.49$ V vs. Fc⁺/Fc (redox couple HL3^{•+}/HL3) was determined in CH₂Cl₂.^[38] Hence, the redox potential of free tBu₂-bq is lower than the redox potentials of the two bisguanidine ligands L1 and L2. Consequently, one expects the oxidised form of the oxolene

ligand, di-tertbutyl-1,2-semiquinone ($t\text{Bu}_2\text{-sq}$), to be stable in the presence of a neutral bisguanidine ligand in its reduced redox state. On the other hand, the redox potential of tetrachloro-1,2-benzoquinone ($\text{Cl}_4\text{-bq}$) is close to those of the bisguanidines, and therefore the redox states of the bisguanidine and oxolene-type ligands within the complex are barely predictable.

Results and Discussion

Complexes with bisguanidines L1 and L2

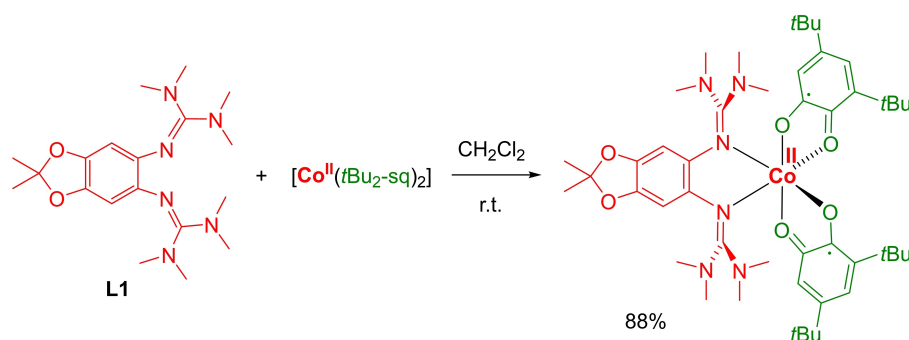
First, the tetrameric complex $[\text{Co}(t\text{Bu-sq})_2]_4$, with bridging semiquinonato ligands, was prepared by reaction between $[\text{Co}_2(\text{CO})_8]$ and $t\text{Bu}_2\text{-bq}$.^[50] Reaction was carried out in CH_2Cl_2 solution instead of benzene used in the literature protocol.^[44] The complex $[\text{Co}(\text{Cl}_4\text{-sq})_2]\cdot\text{CH}_2\text{Cl}_2$ was obtained in a similar way from $[\text{Co}_2(\text{CO})_8]$ and $\text{Cl}_4\text{-bq}$, also in CH_2Cl_2 solution. According to the literature,^[44] the synthesis of this complex is not possible in benzene solution, because it decomposes in this solvent; the authors isolated hexachloro-2,3-oxanthrenequinone as one of the decomposition products. On the other hand, we obtained $[\text{Co}(\text{Cl}_4\text{-sq})_2]\cdot\text{CH}_2\text{Cl}_2$ as a stable product from CH_2Cl_2 solutions. Presumably, the complex is present as oligomer with bridging semiquinonato ligands, like $[\text{Co}(t\text{Bu-sq})_2]_4$,^[44] but it was not possible to grow crystals of sufficient quality for a structural analysis with SCXRD.

Then, the complex $[\text{Co}(t\text{Bu-sq})_2]_4$ was reacted with one of the bisguanidines L1 and L2 in CH_2Cl_2 solutions, giving two new mononuclear complexes in yields of 88% and 82%, respectively, in which cobalt is presumably octahedrally coordinated by two oxolene and one bisguanidine ligands. The product complexes turned out to exhibit high solubility in non-polar as well as polar solvents. For example, while the two reactants, the free bisguanidine (L1 or L2) and $[\text{Co}(t\text{Bu-sq})_2]_4$, are insoluble in *n*-pentane, the produced complexes are highly soluble in this solvent. In the following, we will show that the complexes are best described as *high-spin* Co^{II} complexes with two radical $t\text{Bu}_2\text{-sq}$ ligands and one neutral bisguanidine ligand, $[\text{Co}^{\text{II}}(t\text{Bu}_2\text{-sq})_2(\text{L1})]$ and $[\text{Co}^{\text{II}}(t\text{Bu}_2\text{-sq})_2(\text{L2})]$, as illustrated exemplarily for the complex with L1 in Scheme 2.

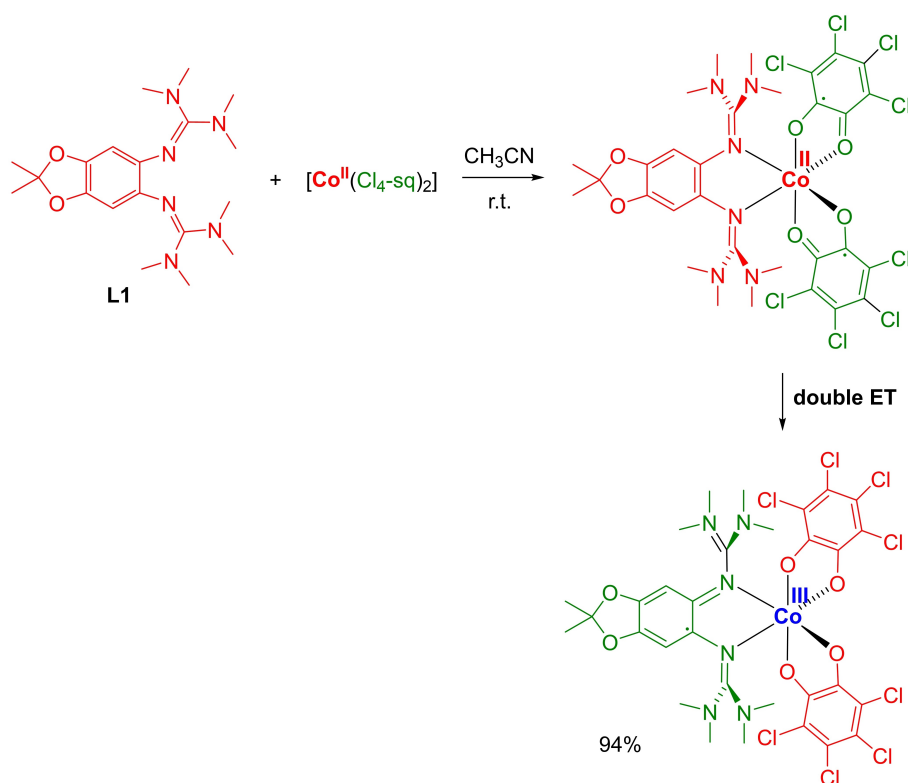
Similarly, mononuclear complexes in which cobalt is octahedrally coordinated by two oxolene and one bisguanidine ligands were obtained as products of the reaction between $[\text{Co}(\text{Cl}_4\text{-sq})_2]$ and one of the bisguanidines L1 or L2. Due to the poor solubility of these product complexes in solvents of low polarity, it was possible to grow crystals suitable for a structural characterization by single-crystal X-ray diffraction (SCXRD). The analysis detailed below shows that the complexes are *low-spin* Co^{III} complexes with two dianionic catecholato ligands and one radical monocationic bisguanidine ligand, $[\text{Co}(\text{Cl}_4\text{-cat})_2(\text{L1})]$ and $[\text{Co}(\text{Cl}_4\text{-cat})_2(\text{L2})]$; see Scheme 3 for the complex with L1. Hence, the higher electron-acceptor character of $\text{Cl}_4\text{-bq}$ compared to $t\text{Bu}_2\text{-bq}$ leads to a different electronic structure, with Co^{III} instead of Co^{II} and a bisguanidine ligand unit in its intermediate radical-monocationic redox state instead of the reduced, neutral one. According to Scheme 3, the reaction between the bisguanidine (L1 or L2) and $[\text{Co}(\text{Cl}_4\text{-sq})_2]$ could formally be divided in two steps. In the first step, complexation leads to a Co^{II} complex with two radical $\text{Cl}_4\text{-sq}$ units similar to the product complexes with $t\text{Bu}_2\text{-sq}$ ligands. Then, intramolecular electron transfer from cobalt to one $\text{Cl}_4\text{-sq}$ unit and from the bisguanidine ligand to the other $\text{Cl}_4\text{-sq}$ unit occurs, leading to cobalt oxidation and formation of a Co^{III} complex with two catecholato ($\text{Cl}_4\text{-cat}$) ligands and a radical monocationic bisguanidine ligand. In summary, the results show that the electronic structure could be changed by modifying the oxolene co-ligands without altering the coordination mode. In the following, we will present and discuss the analytical data that was used to disclose the electronic structures.

Single-crystal X-ray crystallography

The complex $[\text{Co}(\text{Cl}_4\text{-cat})_2(\text{L1})]$ was crystallised by diffusion of pentane into a saturated solution of 1,2-difluorobenzene, and the complex $[\text{Co}(\text{Cl}_4\text{-cat})_2(\text{L2})]$ was crystallised by diffusion of Et_2O into a saturated dimethylformamide solution. Figure 1 illustrates the structures in the solid state, and selected bond lengths are collected in Table 1. The Co-N and Co-O bond lengths, measuring in average 1.953 and 1.902 Å, respectively, for $[\text{Co}(\text{Cl}_4\text{-cat})_2(\text{L1})]$ and 1.946 and 1.903 Å, respectively, for $[\text{Co}(\text{Cl}_4\text{-cat})_2(\text{L2})]$, fall in typical ranges for bonds involving *low-*



Scheme 2. Reaction of $[\text{Co}(t\text{Bu}_2\text{-sq})_2]$ with L1 to give the *high-spin* Co^{II} complex $[\text{Co}(t\text{Bu}_2\text{-sq})_2(\text{L1})]$ with neutral bisguanidine ligand. Bisguanidine L2 reacts similarly.



Scheme 3. Formal partition of the reaction between L1 and $[\text{Co}(\text{Cl}_4\text{-sq})_2]$ into a ligand addition step and an electron transfer (ET) step, leading eventually to the *low-spin* Co^{III} complex $[\text{Co}(\text{Cl}_4\text{-cat})_2(\text{L1})]$ with radical monocationic bisguanidine ligand. Bisguanidine L2 reacts similarly.

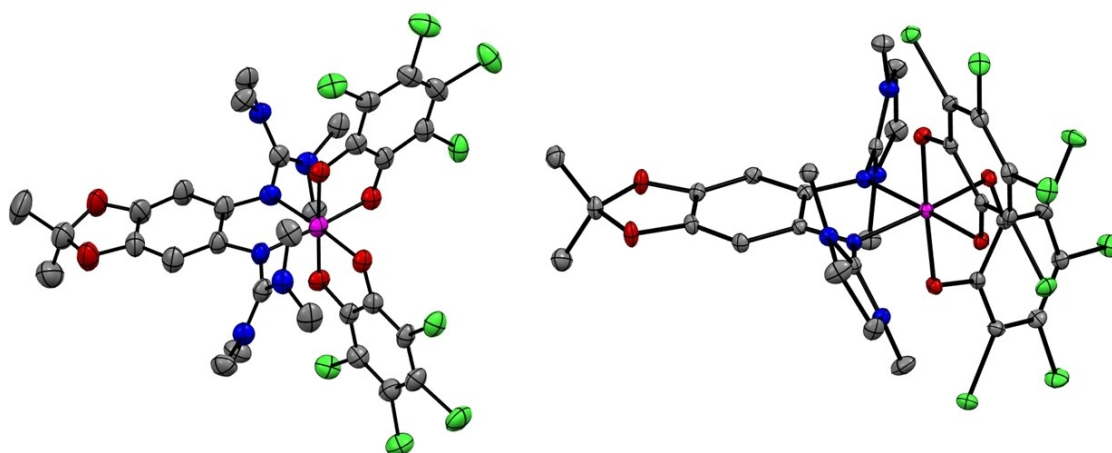


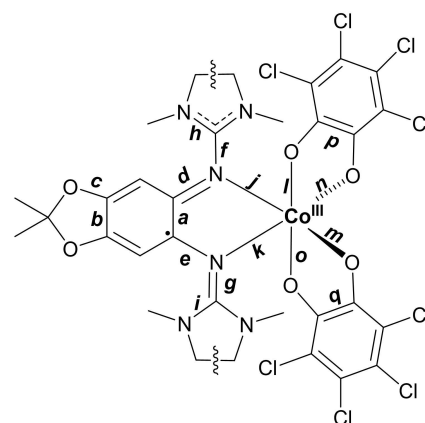
Figure 1. Illustration of the solid-state structures of $[\text{Co}(\text{Cl}_4\text{-cat})_2(\text{L1})]$ and $[\text{Co}(\text{Cl}_4\text{-cat})_2(\text{L2})]$. Co-crystallised solvent molecules and hydrogen atoms are omitted. Displacement ellipsoids are drawn at the 50% probability level. Colour code: Co pink, C grey, O red, N blue, Cl green.

spin Co^{III} .^[34,35,51,52] They are significantly shorter than typical Co-N and Co-O bonds involving *high-spin* Co^{II} , measuring in average 2.17(3) and 2.04(2) Å, respectively, according to a CCDC survey.^[45] The significant variations in the C–C bond lengths within the C_6 ring of the bisguanidine ligands, ranging from 1.348(9) to 1.460(8) Å in $[\text{Co}(\text{Cl}_4\text{-cat})_2(\text{L1})]$ and 1.364(2) to 1.452(2) Å in $[\text{Co}(\text{Cl}_4\text{-cat})_2(\text{L2})]$, indicate loss of aromaticity. The former C=N imino double bond lengths, measuring 1.295(1)/

1.292(1) Å in L1 and 1.293(2)/1.287(2) Å in L2,^[36] increase to 1.384(7)/1.399(7) Å in $[\text{Co}(\text{Cl}_4\text{-cat})_2(\text{L1})]$ and 1.375(2)/1.380(2) Å in $[\text{Co}(\text{Cl}_4\text{-cat})_2(\text{L2})]$, indicating oxidation of the bisguanidine ligands to their radical monocationic redox state.^[34,36,39] Using the correlation between bond lengths and oxidation states established by Brown for oxolenes and related ligands,^[53] we arrive at “metrical oxidation states” (MOS values) for the two $\text{Cl}_4\text{-sq}$ ligands in $[\text{Co}(\text{Cl}_4\text{-cat})_2(\text{L1})]$ and $[\text{Co}(\text{Cl}_4\text{-cat})_2(\text{L2})]$ of

Table 1. Selected bond lengths (in Å) for the two cobalt complexes [Co(Cl₄-cat)₂(L1)] and [Co(Cl₄-cat)₂(L2)].

bond	[Co(Cl ₄ -cat) ₂ (L1)]	[Co(Cl ₄ -cat) ₂ (L2)]
a	1.460(8)	1.452(2)
b	1.396(9)	1.414(3)
c	1.354(8)	1.352(2)
d/e	1.364(7)/1.355(8)	1.356(2)/1.348(2)
f/g	1.384(7)/1.399(7)	1.375(2)/1.380(2)
h/i	1.328(8)/1.311(8)	1.336(2)/1.312(2)
j/k	1.971(5)/1.935(5)	1.954(2)/1.938(2)
l	1.902(4)	1.914(2)
m	1.912(4)	1.891(2)
n	1.906(4)	1.907(2)
o	1.886(4)	1.898(2)
p/q	1.418(9)/1.423(8)	1.427(2)/1.428(2)



−1.82 ± 0.11 and −1.67 ± 0.12, respectively. Hence, the structural data are in line with the formulation as catecholato ligands. Unfortunately, no structural information is available for the complexes [Co^{II}(tBu₂-sq)₂(L1)] and [Co^{II}(tBu₂-sq)₂(L2)]. Because of the high solubility of both complexes in polar and nonpolar solvents, it was not possible to grow single crystals suitable for SCXRD.

Magnetometric (SQUID) measurements

Figure 2 compares the results of the magnetometric (superconductive quantum interference device (SQUID)) measurements for the four complexes [Co(tBu₂-sq)₂(L1)], [Co(tBu₂-sq)₂(L2)], [Co(Cl₄-cat)₂(L1)] and [Co(Cl₄-cat)₂(L2)]. At 300 K, complexes [Co(tBu₂-sq)₂(L1)] and [Co(tBu₂-sq)₂(L2)] exhibit quite large χT values of 3.12 and 3.44 cm³ K mol^{−1}, respectively, in line with the presence of *high-spin* Co^{II} (three metal-centered

and two ligand-centered unpaired electrons). For a non-coupled system without spin-orbit coupling, one would expect a lower χT value of 2.63 cm³ K mol^{−1} (1.875 + 2 · 0.375 = 2.63), confirming the significant spin-orbit coupling typical for octahedral Co^{II} complexes. The χT value remains high with decreasing temperature until ca. 50 K. At lower temperature it decreases, reaching 2.31 cm³ K mol^{−1} for [Co(tBu₂-sq)₂(L1)] and 2.38 cm³ K mol^{−1} for [Co(tBu₂-sq)₂(L2)] at 2 K. On the other hand, much smaller χT values were measured for the complexes with Cl₄-cat ligands; 0.97 cm³ K mol^{−1} for [Co(Cl₄-cat)₂(L1)] and 0.84 cm³ K mol^{−1} for [Co(Cl₄-cat)₂(L2)] at 300 K. These low values are in line with the presence of a *low-spin* Co^{III} complex with one ligand-centered unpaired electron, for which the Curie law predicts a spin-only χT value of 0.38 cm³ K mol^{−1}. The larger experimental values point to the delocalization of the spin density onto the metal, leading to a significant orbit component. This is further supported by the coupling of the organic radical to the ⁵⁹Co nucleus observed in the EPR spectra of these compounds. Moreover, the temperature-independent paramagnetism (TIP) in Co^{III} complexes might contribute. The χT values of [Co(Cl₄-cat)₂(L1)] and [Co(Cl₄-cat)₂(L2)] first slightly rise with decreasing temperature, but decrease below 10 K, eventually reaching 0.86 and 0.82 cm³ K mol^{−1}, respectively, at 2 K. All these results are fully consistent with the Lewis structures drawn in Scheme 3.

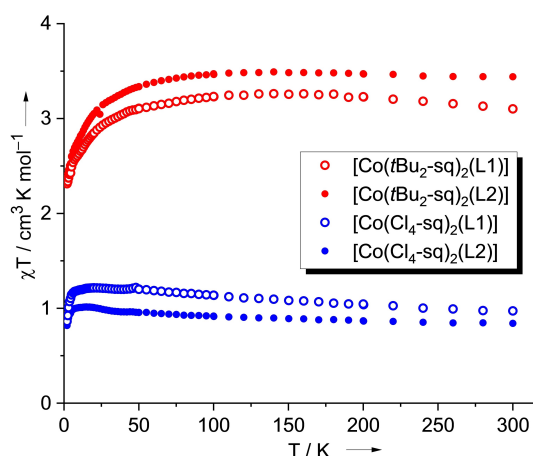


Figure 2. Plot of the magnetometric (SQUID) data (at 50 mT) for the *high-spin* Co^{II} complexes [Co(tBu₂-sq)₂(L1)] and [Co(tBu₂-sq)₂(L2)] (red curves) and the *low-spin* Co^{III} complexes [Co(Cl₄-cat)₂(L1)] and [Co(Cl₄-cat)₂(L2)] (blue curves).

EPR spectroscopy

EPR spectra for [Co(tBu₂-sq)₂(L1)] in CH₂Cl₂ and [Co(Cl₄-cat)₂(L2)] in CH₃CN at 10 K (blue) and at room temperature (red) are reproduced in Figure 3. In the case of [Co(tBu₂-sq)₂(L1)], a weak and broad signal, centered at g = 2.0, was observed in the spectrum at 10 K, showing no hyperfine coupling. At room temperature the signal becomes much sharper. A splitting of the signal into two components is then visible (see zoom into the region around 3430 G, Figure 3), which might arise from zero field splitting (ZFS), due to the presence of two unpaired electrons on the ligand units. From the signal spacings, the

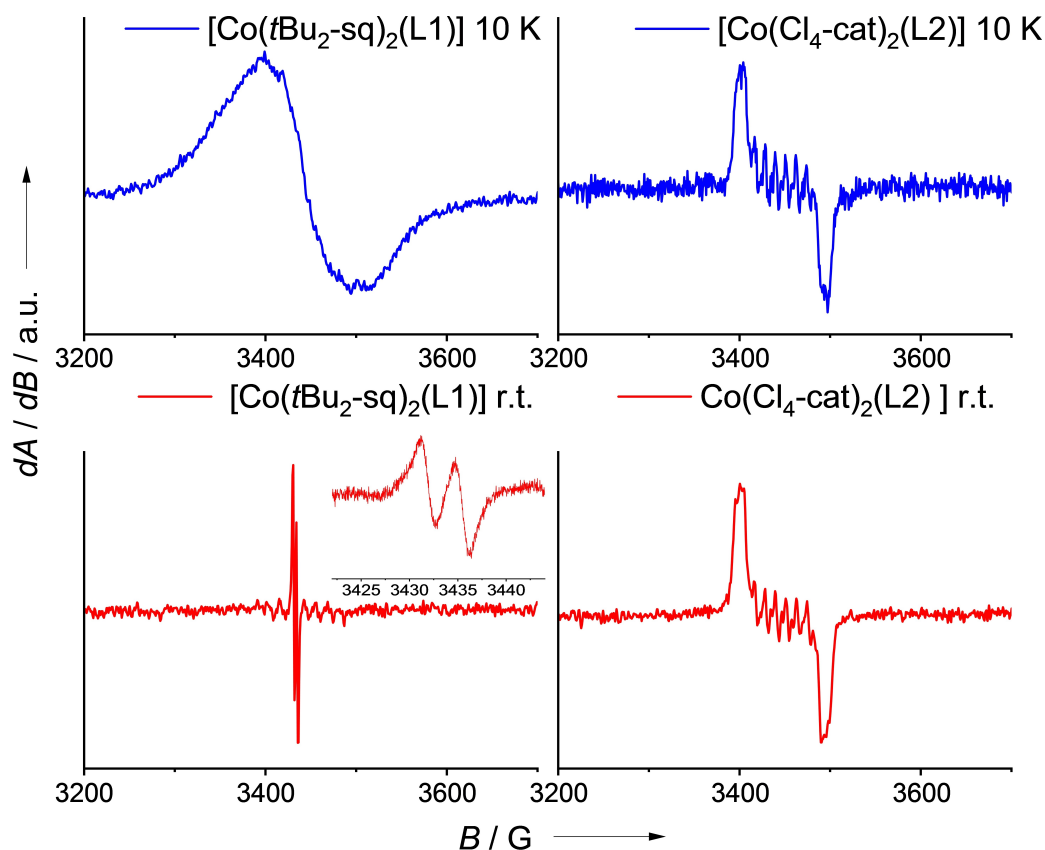


Figure 3. X-band EPR spectra (9.63 GHz) of $[\text{Co}(\text{tBu}_2\text{-sq})_2(\text{L1})]$ in CH_2Cl_2 at 10 K (blue) and room temperature (red) (left) and $[\text{Co}(\text{Cl}_4\text{-cat})_2(\text{L2})]$ in CH_3CN at 10 K (blue) and room temperature (red) (right). The inset above the spectrum of $[\text{Co}(\text{tBu}_2\text{-sq})_2(\text{L1})]$ at room temperature highlights the signal splitting, presumably arising from zero-field splitting.

zero-field splitting parameter D could be estimated to be about 0.0005 cm^{-1} . The low intensity and the broadening of the signal due to $[\text{Co}(\text{tBu}_2\text{-sq})_2(\text{L1})]$ at low temperature most likely arise from the interaction of the cobalt-centred unpaired electrons with the unpaired electrons on the semiquinone co-ligands. Strong (first-order) spin-orbit coupling in octahedral *high-spin* Co^{II} complexes prohibits the detection of a Co signal at room temperature. Also, at low temperatures no signal due to a Co-centred radical was found, arguing for fast relaxation processes for the cobalt-centered electron spins, in line with a significant interaction with the unpaired electrons on the ligands.

In the case of $[\text{Co}(\text{Cl}_4\text{-cat})_2(\text{L2})]$, hyperfine coupling to the ^{59}Co nucleus ($I=7/2$), leads to splitting into eight lines with a hyperfine coupling constant of $A = 12 \text{ G}$. The spectrum recorded at room temperature looks similar to that at 10 K. The observation of this pattern proves partial delocalisation of the spin density from the ligand to the metal. In summary, the EPR spectra clearly show the presence of radical ligands attached to cobalt in all complexes, in line with the Lewis structures sketched in Schemes 2 and 3.

UV-vis spectroscopy

Green solutions formed when the complexes $[\text{Co}(\text{tBu}_2\text{-sq})_2(\text{L1})]$ and $[\text{Co}(\text{tBu}_2\text{-sq})_2(\text{L2})]$ were dissolved in CH_2Cl_2 or other organic solvents. By contrast, solutions of $[\text{Co}(\text{Cl}_4\text{-cat})_2(\text{L1})]$ and $[\text{Co}(\text{Cl}_4\text{-cat})_2(\text{L2})]$ were dark-blue-violet, respectively (see photos embedded in Figure 4a). The UV-vis spectrum of $[\text{Co}(\text{tBu}_2\text{-sq})_2(\text{L1})]$ exhibits three bands at 234 nm, 310 nm and 341 nm (Figure 4a). For $[\text{Co}(\text{tBu}_2\text{-sq})_2(\text{L2})]$, two bands at 229 nm and 338 nm show (Figure 4b). The colour of the solutions arises from broad, unstructured and relatively weak absorptions that extend into the visible region up to ca. 480 nm. The absence of clear signals in the visible region argues for the presence of a neutral guanidine ligand in both complexes, supporting the description of $[\text{Co}(\text{tBu}_2\text{-sq})_2(\text{L1})]$ and $[\text{Co}(\text{tBu}_2\text{-sq})_2(\text{L2})]$ as Co^{II} complexes with neutral bisguanidine ligands. On the other hand, the spectra of $[\text{Co}(\text{Cl}_4\text{-cat})_2(\text{L1})]$ and $[\text{Co}(\text{Cl}_4\text{-cat})_2(\text{L2})]$ (Figure 4a and 4b) exhibit, in addition to a strong band at 247/235 nm, a broad absorption in the visible region centered around 640/580 nm, as well as a band at 366/376 nm (highlighted by an arrow in Figure 4a/4b) characteristic for a bisguanidine unit in its intermediate, radical monocationic redox state.^[36,37] For comparison, the salt $\text{L1}(\text{PF}_6)$ of the un-coordinated radical monocation $\text{L1}^{*\text{+}}$ in CH_3CN solution exhibits a band around 370 nm with a tail extending into the visible region.^[36] The spectrum recorded

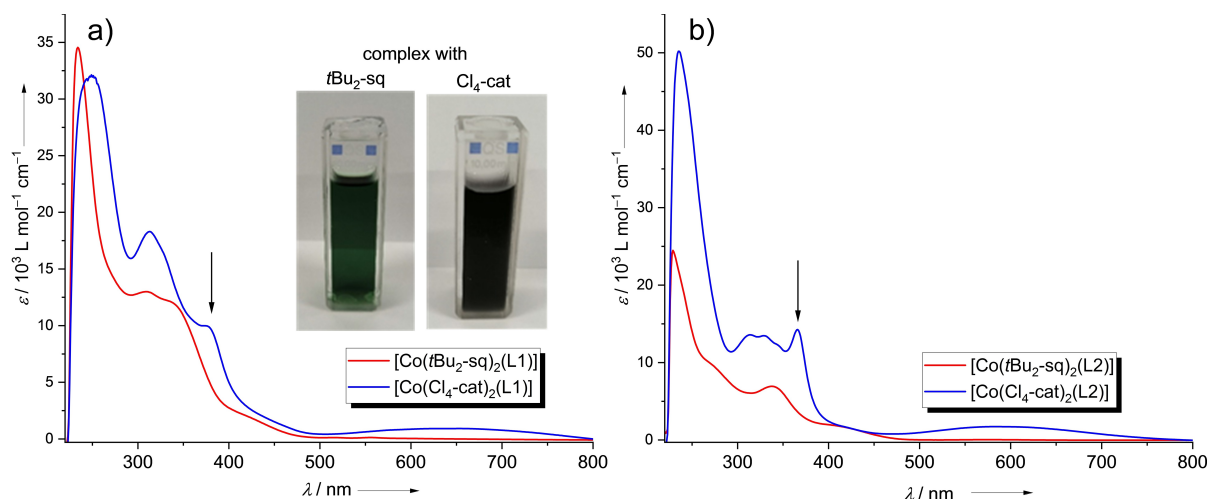


Figure 4. UV-vis spectra of a) $[\text{Co}(\text{tBu}_2\text{-sq})_2(\text{L1})]$ and $[\text{Co}(\text{Cl}_4\text{-cat})_2(\text{L1})]$, and b) $[\text{Co}(\text{tBu}_2\text{-sq})_2(\text{L2})]$ and $[\text{Co}(\text{Cl}_4\text{-cat})_2(\text{L2})]$ in CH_2Cl_2 solutions. The arrows highlight the bands characteristic for the radical monocationic bisguanidine ligand ($\text{L1}^{+\cdot}$ and $\text{L2}^{+\cdot}$).

for the complex $[\text{Co}(\text{Cl}_4\text{-cat})_2(\text{L1})]$ is also in line with the presence of the radical monocation, $\text{L1}^{+\cdot}$. Hence, bands show at 377 and 364 nm, respectively.^[36,39] Hence, the UV-vis spectra are in full agreement with the results from the EPR measurements and the crystallographic data. Consequently, $[\text{Co}(\text{Cl}_4\text{-cat})_2(\text{L1})]$ and $[\text{Co}(\text{Cl}_4\text{-cat})_2(\text{L2})]$ are best described as Co^{III} complexes with a radical monocationic bisguanidine ligand. The Lewis structures sketched in Schemes 2 and 3 most adequately describe the electronic structures. UV-vis studies at variable temperature (in the range -40°C to $+40^\circ\text{C}$) found no indication for a significant temperature-induced change of the electronic structures. Complexes $[\text{Co}(\text{tBu}_2\text{-sq})_2(\text{L1})]$ and $[\text{Co}(\text{tBu}_2\text{-sq})_2(\text{L2})]$ decomposed at 40°C ; complexes $[\text{Co}(\text{Cl}_4\text{-cat})_2(\text{L1})]$ and $[\text{Co}(\text{Cl}_4\text{-cat})_2(\text{L2})]$ were stable at this temperature but showed no significant variations in the UV-vis spectra. A possible thermal equilibrium between two redox isomers (valence tautomerism) should favour the Co^{III} redox isomer at lower temperature, and the Co^{II} redox isomer at higher temperature. $[\text{Co}(\text{Cl}_4\text{-cat})_2(\text{L1})]$ and $[\text{Co}(\text{Cl}_4\text{-cat})_2(\text{L2})]$ are Co^{III} complexes at room temperature; therefore a thermally-induced valence tautomerism upon cooling is unlikely to happen.

Cyclic Voltammetry

The CV curves of the complexes $[\text{Co}(\text{tBu}_2\text{-sq})_2(\text{L1})]$, $[\text{Co}(\text{tBu}_2\text{-sq})_2(\text{L2})]$, $[\text{Co}(\text{Cl}_4\text{-cat})_2(\text{L1})]$ and $[\text{Co}(\text{Cl}_4\text{-cat})_2(\text{L2})]$ are included in the Supporting Information. All complexes show a series of redox events mostly lacking reversibility, probably due to strong electronic or structural changes. For the complexes $[\text{Co}(\text{tBu}_2\text{-sq})_2(\text{L1})]$ and $[\text{Co}(\text{tBu}_2\text{-sq})_2(\text{L2})]$, the curves indicate reversible reduction at a potential ($E_{1/2}$ value) of -1.04 V vs. Fc^+/Fc , assignable to reduction of one or both of the semiquinonate ligands to the corresponding catecholate.

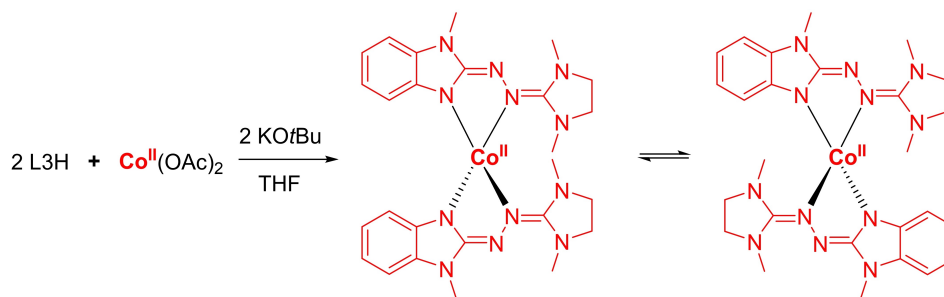
Complexes with urea azine (biguanidine) L3

We now turn to the results obtained with ligand L3^- . Complexes exhibiting both this ligand as well as an oxolene ligand ($\text{Cl}_4\text{-cat}$, $\text{Cl}_4\text{-sq}$ or $\text{Cl}_4\text{-bq}$) could in principle be obtained in two ways, starting either with the up to date unknown complex $[\text{Co}(\text{L3})_2]$ or with $[\text{Co}(\text{Cl}_4\text{-sq})_2]$. In the following we first report the synthesis of $[\text{Co}(\text{L3})_2]$ and its reaction with $\text{Cl}_4\text{-bq}$, and then discuss the results of the reaction between $[\text{Co}(\text{Cl}_4\text{-sq})_2]$ and HL3 (the protonated precursor to ligand L3^-).

Synthesis of the precursor $[\text{Co}(\text{L3})_2]$

Reaction between two equivalents of HL3 and $\text{Co}(\text{OAc})_2$ in the presence of KOtBu gave the homoleptic complex $[\text{Co}(\text{L3})_2]$ in an isolated yield of 54% (Scheme 4). Red crystals of the complex were obtained by layering a saturated CH_2Cl_2 solution with Et_2O . Similar to the analogue copper complex $[\text{Cu}(\text{L3})_2]$,^[38] the crystal structure (Figure 5) shows a *cis*-type conformation of the ligands. The bond lengths within the two azine ligands are in accordance with the reduced form L3^- ,^[38] the coordination mode of the cobalt atom is in between tetrahedral and square-planar, with a smallest angle between the two N–Co–N planes of 56.9° . In solution, an equilibrium between *cis*- and *trans*-type isomers is likely to be established (similar to the results obtained with the analogue copper complex^[38]). According to quantum-chemical calculations (B3LYP/def2-TZVP), the *trans*-isomer is marginally favoured (by 3.8 kJ mol^{-1} for the isolated molecule). As expected, the complex exhibits two short Co–N bond lengths of $1.963(1)/1.950(1)\text{ \AA}$ and two longer ones of $2.017(1)/2.035(1)\text{ \AA}$ (see Table 2).

The EPR (X-band) spectrum of a CH_2Cl_2 solution was free of signals, both at low temperature (7 K) and at room temperature. On the other hand, the room temperature paramagnetic ^1H NMR spectrum in CD_2Cl_2 solution (see Supporting Information)



Scheme 4. Synthesis of the complex $[\text{Co}(\text{L}3)_2]$ from $[\text{Co}(\text{OAc})_2]$ and two equivalents of HL3. The product crystallises in the *cis*-type isomeric form, but *cis*- and *trans*-isomers should be in equilibrium in solution (see also the discussion for the analogue copper complexes in Ref. [38]).

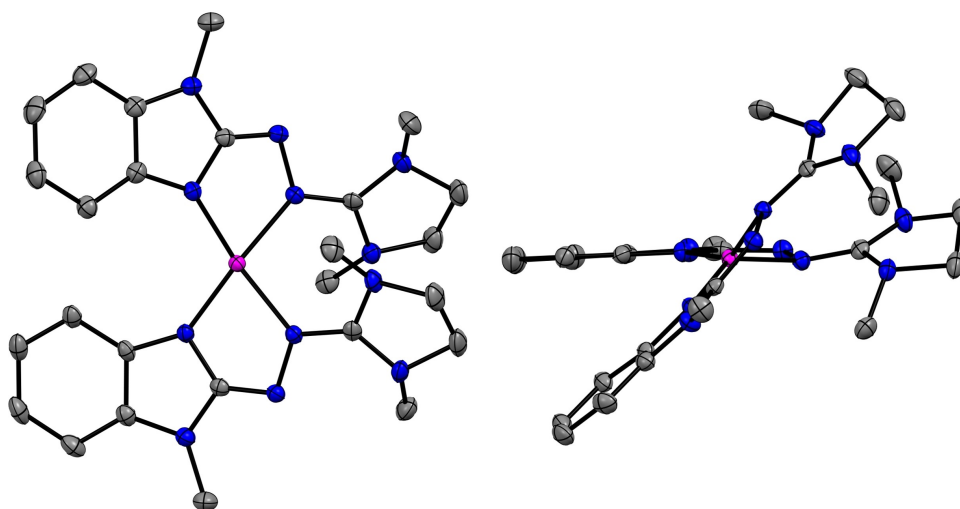
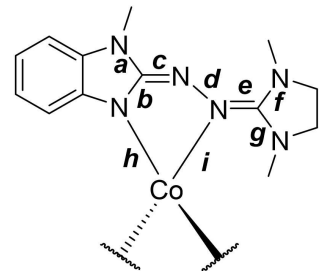


Figure 5. Illustration of the solid-state structure of $[\text{Co}(\text{L}3)_2]$ from two perspectives. Displacement ellipsoids are drawn at the 50% probability level. Hydrogen atoms are omitted. Colour code: Co pink, C grey, N blue.

Table 2. Selected structural parameters (bond lengths in Å, angle in °) for $[\text{Co}(\text{L}3)_2]$ in the solid state.

parameter	bond length/angle
a	1.386(2)/1.385(2)
b	1.372(2)/1.374(2)
c	1.305(2)/1.304(2)
d	1.436(2)/1.431(2)
e	1.310(2)/1.311(2)
f	1.365(2)/1.365(2)
g	1.382(2)/1.384(2)
h	1.963(1)/1.950(1)
i	2.017(1)/2.035(1)
$\angle^* \text{ML}_2$	56.9



* Smallest dihedral angle between the two N–Co–N planes.

shows eleven mostly sharp signals in the range $\delta = 68$ to (-150) ppm, arguing for fast electron relaxation that is responsible for the absence of signals in the EPR spectra, even at low temperatures. Obviously, the observed eleven signals in the ^1H NMR spectrum belong to the eleven different protons of the complex, but an unambiguous assignment was not possible on

the basis of the measured data. We abstained from a more detailed analysis of the paramagnetic NMR spectra.

Additional magnetic measurements in CD_2Cl_2 solution at room temperature with the Evans NMR method^[54,55] resulted in a χT value of $2.67 \text{ cm}^3 \text{ K mol}^{-1}$ (with diamagnetic correction using Pascal constants^[56]), being a typical value for *high-spin* Co^{II} with some degree of spin-orbit coupling.

The UV-vis spectrum (see Supporting Information) contains strong, sharp bands at 284 and 335 nm. In the visible region, only weak and broad bands were visible, with a maximum of absorption at 493 nm and a shoulder at 571 nm. Similar bands were also observed in the neutral $[\text{Cu}(\text{L}1)_2]$ complex.^[28] In addition, a very weak band around 990 nm with a shoulder at 1150 nm appeared; its origin remains unclear.

In Figure 6, the cyclic voltammogram of $[\text{Co}(\text{L}3)_2]$ is compared with those measured previously for the complexes $[\text{Cu}(\text{L}3)_2]$ and $[\text{Zn}(\text{L}3)_2]$.^[38] The observed redox waves for the Co complex are similar to the Zn complex, with two consecutive reversible one-electron redox steps, at $E_{1/2} = -0.61 \text{ V}$ ($E_{\text{ox}} = -0.54 \text{ V}$) and $E_{1/2} = -0.39 \text{ V}$ ($E_{\text{ox}} = -0.32 \text{ V}$), followed by at least one irreversible process, probably due to oxidation-induced decomposition of the complex. The similarity between the

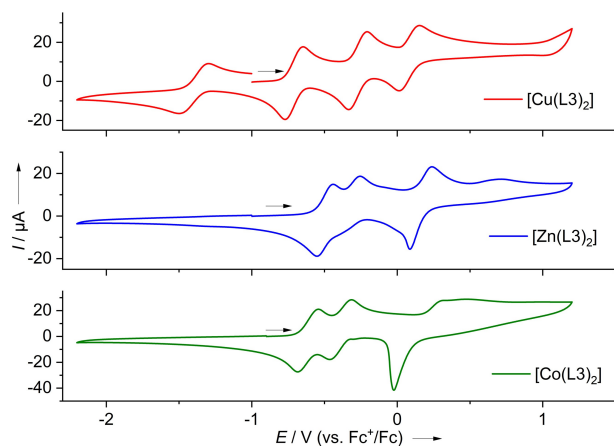


Figure 6. Comparison between the cyclic voltammograms (CV curves) for the three complexes $[\text{Cu}(\text{L}3)_2]$,^[28] $[\text{Zn}(\text{L}3)_2]$ ^[28] and $[\text{Co}(\text{L}3)_2]$ in CH_2Cl_2 solutions (scan rate 100 mV s^{-1} , Ag/AgCl reference electrode, ${}^n\text{Bu}_4\text{PF}_6$ as supporting electrolyte).

observed cyclic voltammograms of the zinc and cobalt complexes indicates that the first two waves belong to ligand-centered one-electron redox processes, leading eventually to a Co^{II} complex with two radical neutral ligands L3.

Reaction of $[\text{Co}(\text{L}3)_2]$ with $\text{Cl}_4\text{-bq}$

We then reacted complex $[\text{Co}(\text{L}3)_2]$ with $\text{Cl}_4\text{-bq}$ in a 1:1 ratio. Unfortunately, it was not possible to isolate a clean product, but a few crystals of one of the products suitable for a structural analysis by SCXRD precipitated from the reaction mixture. This product turned out to be the salt $[\text{H}_2\text{L}3]^+[\text{Co}^{\text{III}}(\text{L}3)(\text{Cl}_4\text{-cat})_2]^-$, the anion being a Co^{III} complex with a radical, neutral azine ligand $\text{L}3^*$ and two catecholato ligands. Previous work on urea azine complexes showed that the ethylene bridge between the two N atoms is amenable to deprotonation,^[57] explaining the presence of the protonated ligand, $[\text{H}_2\text{L}3]^+$, as counterion. Crystals were

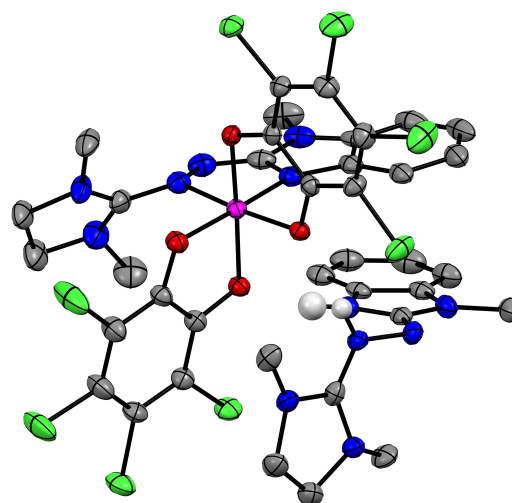


Figure 7. Illustration of the solid-state structure of $[\text{H}_2\text{L}3]^+[\text{Co}^{\text{III}}(\text{L}3)(\text{Cl}_4\text{-cat})_2]^-$. Only one ion pair is shown. Displacement ellipsoids are drawn at the 50% probability level. Hydrogen atoms except for N-H are omitted. Colour code: Co pink, C grey, N blue, O red, Cl green, H pale grey.

grown by layering a concentrated solution of the raw product in CH_2Cl_2 with *n*-hexane. Figure 7 illustrates the structure in the solid state, and Table 3 contains selected bond lengths and angles. The cobalt atom is octahedrally coordinated. The four Co–O bond lengths (1.890(2), 1.901(3), 1.920(2) and 1.897(2) Å) clearly argue for the presence of low-spin Co^{III} .^[45,46] An estimation of the metrical oxidation state (MOS)^[47] of the two $\text{Cl}_4\text{-cat}$ units resulted in a MOS of -1.82 ± 0.15 and -1.76 ± 0.12 respectively. With 1.364(4) Å, the central N–N bond (N1–N4) of the coordinated azine unit is significantly shorter than the central N–N bond (N7–N10) in the cation $[\text{H}_2\text{L}3]^+$ (1.423(4) Å), arguing for some double-bond character. The bond parameters indicate that the azine ligand is in its neutral radical redox state, $\text{L}3^*$. Unfortunately, it was not possible to isolate a larger amount of pure compound; therefore, no further analytical data were measured. Nevertheless, the results are useful as they show that

Table 3. Selected bond lengths (in Å) for $[\text{H}_2\text{L}3]^+[\text{Co}^{\text{III}}(\text{L}3)(\text{Cl}_4\text{-cat})_2]^-$ in the solid state.

bond	$[\text{Co}^{\text{III}}(\text{L}3)(\text{Cl}_4\text{-cat})_2]^-$	$[\text{H}_2\text{L}3]^+$
a	1.357(4)	1.372(4)
b	1.344(5)	1.359(5)
c	1.337(5)	1.311(4)
d	1.364(4)	1.423(4)
e	1.370(5)	1.311(4)
f	1.320(5)	1.361(4)
g	1.337(5)	1.347(4)
h	1.902(2)	
i	1.949(3)	
j	1.890(2)	
k	1.901(3)	
l	1.920(2)	
m	1.897(2)	
n	1.419(4)	
o	1.417(4)	

the urea azine is oxidised and the benzoquinone ($\text{Cl}_4\text{-bq}$) reduced.

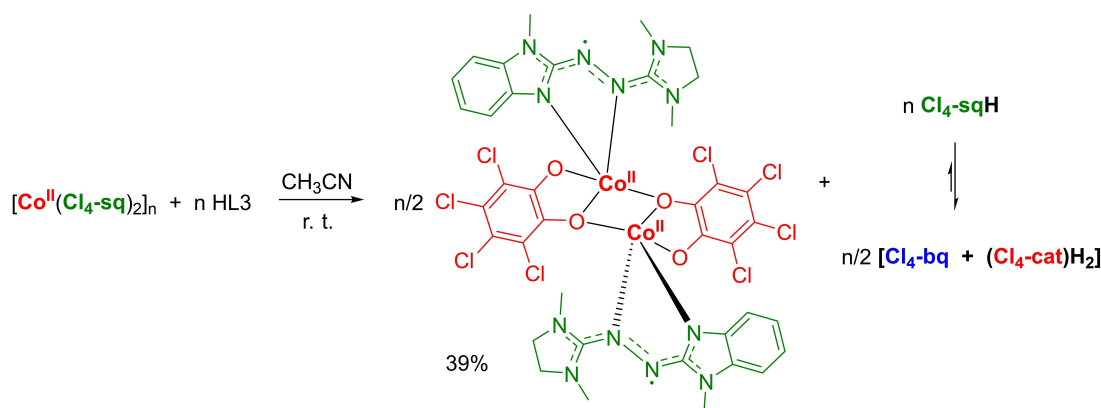
Reaction of $[\text{Co}(\text{Cl}_4\text{-sq})_2]$ with HL3

Finally, we reacted $[\text{Co}(\text{Cl}_4\text{-sq})_2]$ with the protonated precursor HL3. Surprisingly, the dinuclear complex $[\text{Co}_2(\text{Cl}_4\text{-cat})_2(\text{L3})_2]$ was obtained as product, in a crystal yield of 39% (Scheme 5). By contrast, the same reaction conditions produce mononuclear complexes in the case of reactions with L1 and L2 (Scheme 3). The formation of the dinuclear complex is most likely caused by the (postulated) oligomeric nature of the $[\text{Co}(\text{Cl}_4\text{-sq})_2]$ starting complex (see discussion above). In this complex, two *high-spin* Co^{II} atoms are bound to two catecholato ligands and two radical neutral urea azine ligands, L3^\bullet . The HL3 reactants are deprotonated and replace half of the $\text{Cl}_4\text{-sq}$ ligands. The eliminated, protonated semiquinonate molecules ($\text{Cl}_4\text{-sqH}$) should be in a disproportionation equilibrium with $\text{Cl}_4\text{-bq}$ and

$(\text{Cl}_4\text{-cat})\text{H}_2$. In this context we like to mention that studies from Heyduk *et al.* showed that neutral imino-semiquinone radicals are stable toward disproportionation, while ortho-semiquinone radicals usually disproportionate.^[58] Therefore, in our reaction (Scheme 5) the equilibrium should lie almost completely on the side of $(\text{Cl}_4\text{-cat})\text{H}_2$ and $\text{Cl}_4\text{-bq}$. Finally, the oxolene units that remain attached to the Co are reduced from $\text{Cl}_4\text{-sq}$ to $\text{Cl}_4\text{-cat}$, and the L3^\bullet is oxidised to the intermediate, radical redox state, L3^\bullet . In the following, we discuss the analytical data that was used for the evaluation of the electronic structure.

Single-crystal X-ray diffractometry

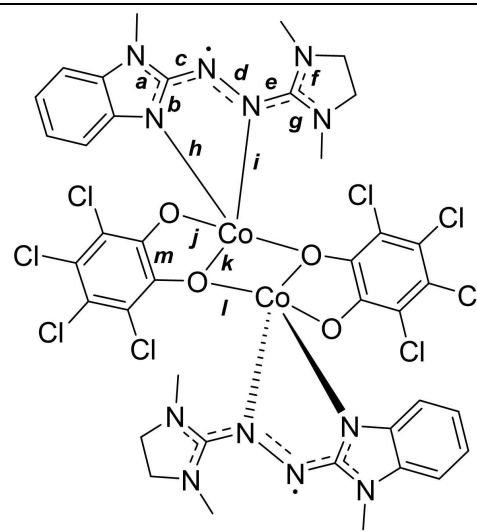
Crystals of sufficient quality for a structural characterization with SCXRD were obtained by gas-phase diffusion of Et_2O into a saturated CH_3CN solution. Figure 8 illustrates the structure; selected bond lengths are included in Table 4. The two $\text{Cl}_4\text{-cat}$ units bridge the two Co atoms, the bridging O atoms (O2 and



Scheme 5. Reaction between $[\text{Co}(\text{Cl}_4\text{-sq})_2]_n$ and HL3 to give the new dinuclear complex $[\text{Co}_2(\text{Cl}_4\text{-cat})_2(\text{L3})_2]$.

Table 4. Selected bond lengths (in Å) for $[\text{Co}_2(\text{Cl}_4\text{-cat})_2(\text{L3})_2] \cdot 2\text{CH}_3\text{CN}$ in the solid state.

bond	$[\text{Co}_2(\text{Cl}_4\text{-cat})_2(\text{L3})_2]$
a	1.369(2)/1.367(2)
b	1.350(2)/1.347(2)
c	1.337(2)/1.342(2)
d	1.361(1)/1.364(2)
e	1.357(2)/1.359(2)
f	1.344(2)/1.344(2)
g	1.345(2)/1.336(2)
h	1.989(1)/1.981(1)
i	2.190(1)/2.142(1)
j	1.946(1)/1.956(1)
k	2.179(1)/2.219(1)
l	2.014(1)/1.999(1)
m	1.425(2)/1.430(2)



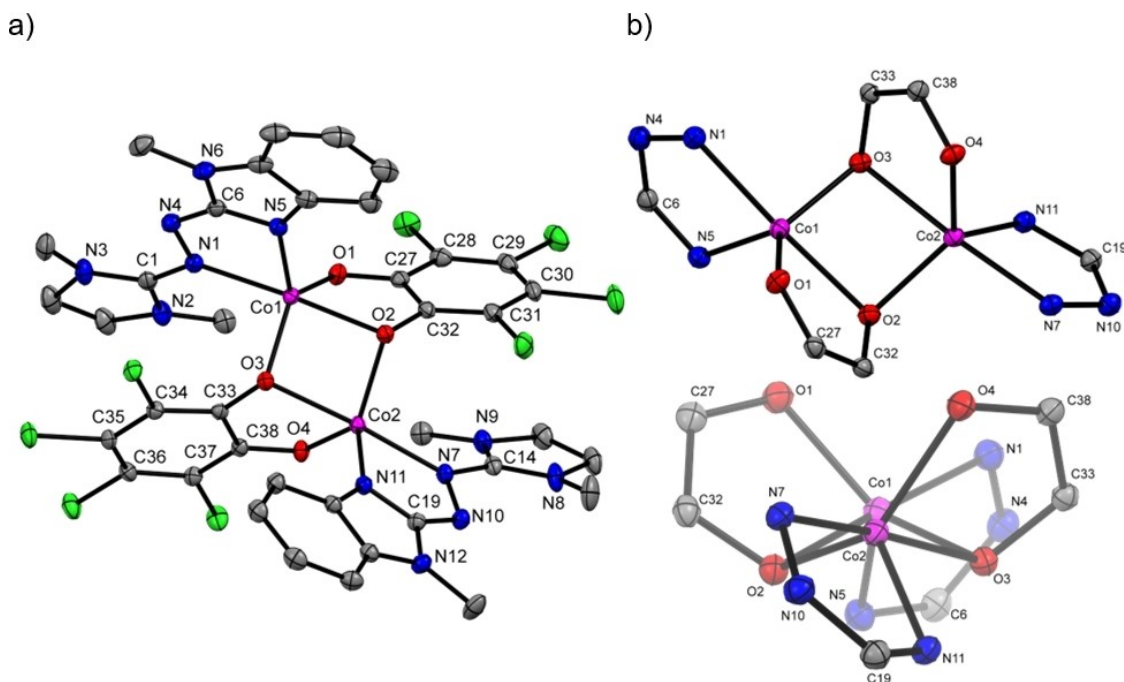


Figure 8. a) Illustration of the solid-state structure of the dinuclear Co^{II} complex $[\text{Co}_2(\text{Cl}_4\text{-cat})_2(\text{L3})_2]$. The co-crystallised two CH_3CN solvent molecules and all hydrogen atoms are omitted. Displacement ellipsoids are drawn at the 50% probability level. Colour code: Co pink, C grey, O red, N blue, Cl green. b) Representations highlighting the Co coordination mode from two perspectives.

O3) being bound slightly unsymmetrically, with Co–O distances of 2.179(1)/2.014(1) Å (Co1–O2/Co2–O2) and 1.999(1)/2.219(1) Å (Co1–O3/Co2–O3). The shortest Co–O bonds involve oxygen atoms (O1 and O4) that are only bound to one cobalt atom (1.946(1)/1.956(1) Å). The Co···Co separation of 3.0282(5) Å indicates the absence of a significant direct metal-metal bond. By analysis of the structural parameters within each ligand type, their respective redox states can be assigned. First of all, the structures of the two urea azine ligands are similar, indicating that they have similar oxidation states. Also, the structures of the two catecholato ligands are similar. For the urea azine ligands, the bond lengths within the central CNNC unit serve as valuable indicator for the redox state.^[34] The respective bond lengths are 1.357(2)/1.359(2) Å for the former C=N imino bonds (C1–N1/N7–C14), 1.361(1)/1.364(2) Å for the central N–N bonds (N1–N4/N7–N10), and 1.337(2)/1.342(2) Å for the second CN imino bonds (N4–C6/N10–C19). For comparison, the corresponding bond lengths of the free, protonated ligand HL3 are 1.295, 1.424, and 1.295 Å, respectively.^[38] The harmonization of the bond lengths, i.e. the elongation of the former C=N double bonds and shortening of the central N–N bond caused by charge delocalisation within the urea azine unit, indicates the presence of the radical neutral redox state, L3^{\cdot} . By contrast, the former $\text{Cl}_4\text{-sq}$ ligands show bond lengths that are in accordance with the fully reduced catecholato form. In particular, the similarity of the C–C bond lengths within the C_6 ring (1.389, 1.381, 1.391, 1.378, 1.399 and 1.372 Å) indicate the presence of an intact aromatic system.^[59] Estimation of the metrical oxidation state (MOS)^[47] for the two $\text{Cl}_4\text{-sq}$ units resulted in a MOS of -1.75 ± 0.12 and -1.69 ± 0.12 , respectively. Conse-

quently, an oxidation state +II could be assigned to both cobalt atoms.

The fivefold coordination mode of the cobalt atoms can be described as distorted trigonal-bipyramidal, which is reflected by the τ values (zero for perfectly tetragonal geometry and unity for a perfectly trigonal-bipyramidal geometry)^[60] of 0.77 (Co1) and 0.82 (Co2) respectively. The ligand atoms O1, O3 and N5 are bound to Co1, and N11, O2 and O4 are bound to Co2 in equatorial positions, and N1 and O2 for Co1, and N7 and O3 for Co2 in axial positions. The two N donor atoms of each azine ligand are very differently bound, with one short Co–N bond (N5–Co1/N11–Co2) of 1.989(1)/1.981(1) Å, and a significantly longer one (N1–Co1/N7–Co2) of 2.190(1)/2.142(1) Å. Also, for the bridging $\text{Cl}_4\text{-catecholato}$ ligands one short Co–O bond (Co1–O1/Co2–O4) of 1.946(1)/1.956(1) Å, and two elongated Co–O bonds (Co1–O2/Co1–O3 and Co2–O2/Co2–O3) of 2.179(1)/1.999(1) Å and 2.014(1)/2.219(1) Å, respectively, were found.

EPR spectroscopy

X-band EPR spectra, recorded in frozen CD_2Cl_2 at 7 K, show a signal close to the free electron g value (see Supporting Information). The EPR experiment did not show a cobalt centred radical signal probably due to fast electron relaxation via intramolecular exchange processes. The (paramagnetic) ^1H NMR spectrum at room temperature shows several sharp signals, arguing for a fast relaxation process that prohibits the detection of signals in the EPR spectrum. The EPR and NMR spectra show

the presence of radical ligands in the complex, in line with the Lewis structure sketched in Scheme 5.

UV-vis spectroscopy

The UV-vis spectrum of the intensively pink complex in CH_3CN (Figure 9) contains three bands at 509, 339 and 223 nm; the intense low energy band is characteristic for the radical neutral form of the azine ligand, L3^{\bullet} . The spectrum resembles the one observed for $[\text{Cu}(\text{L3})_2]\text{PF}_6$ (apart from the IR intervalence band observed in the copper complex)^[38] featuring two neutral, radical L3^{\bullet} ligands and a Cu^{I} atom.^[38] Hence, the UV-vis spectrum supports the electronic description derived from the SCXRD data, and is in line with the Lewis structure shown in Scheme 5.

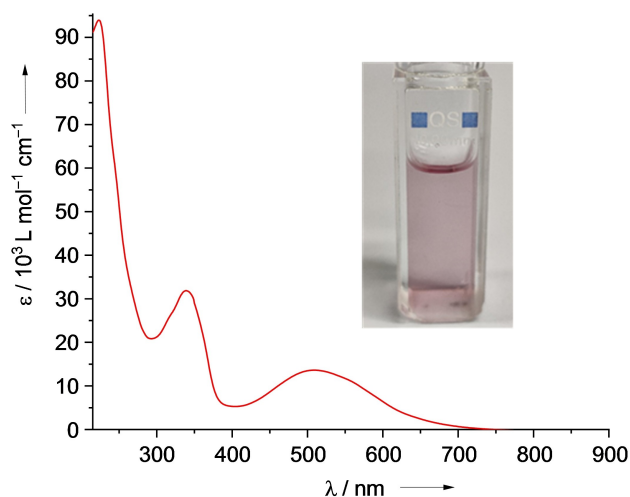


Figure 9. UV-vis spectrum of $[\text{Co}_2(\text{Cl}_4\text{-cat})_2(\text{L3})_2]$ in CH_3CN solution ($c = 1.55 \cdot 10^{-5} \text{ mol} \cdot \text{l}^{-1}$). A photo of the solution is embedded.

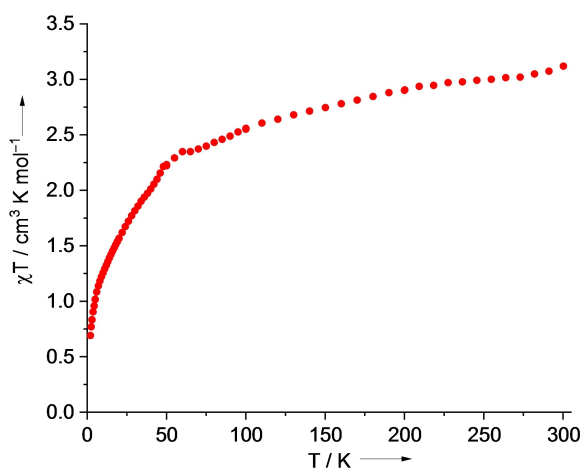


Figure 10. Plot of the magnetometric (SQUID) data (at 50 mT) for solid $[\text{Co}_2(\text{Cl}_4\text{-cat})_2(\text{L3})_2]$.

Magnetometric (SQUID) measurements

Magnetometric (SQUID) measurements carried out for the complex in the solid state (Figure 10) found a χT value of $3.14 \text{ cm}^3 \text{ K mol}^{-1}$ at 300 K. This value is in good agreement with $\chi T = 2.99 \text{ cm}^3 \text{ K mol}^{-1}$ at 298 K obtained in solution by ^1H NMR spectroscopy using the Evans method (CD_2Cl_2). For a hypothetical non-coupled dimeric complex with two *high-spin* Co^{II} atoms and two organic radical ligands, L3^{\bullet} , one expects a spin-only χT value of $4.5 \text{ cm}^3 \text{ K mol}^{-1}$ ($(2 \cdot 1.875 + 2 \cdot 0.375) \text{ cm}^3 \text{ K mol}^{-1}$). Due to significant orbit contributions from the *high-spin* Co^{II} atoms, the actual value should be even higher. Hence, the lower experimental value (both in solution and in the solid state) argues for significant antiferromagnetic interactions between the spin centers.

In the solid state, the χT value decreases with decreasing temperature, first slowly until ca. 50 K ($\chi T = 2.3 \text{ cm}^3 \text{ K mol}^{-1}$), and then rapidly, reaching $0.73 \text{ cm}^3 \text{ K mol}^{-1}$ at 2 K, in line with dominating antiferromagnetic coupling.

Quantum-chemical calculations

To obtain further information, quantum-chemical (DFT) calculations were carried out on the basis of the broken-symmetry description. In these calculations, we used the B3LYP functional in combination with the def2-TZVP basis set. This method was shown previously to give quite reliable results for some complexes,^[61] including cobalt complexes with redox-active guanidines.^[34,35,38] Generally, DFT methods have to be treated with caution when applied to open-shell molecules such as cobalt complexes.^[62,63] On the other hand, multireference calculations (such as NEVPT2 or CASSCF) are not simple for molecules of that size.

The calculations found a ^9A state ($S_z = 4$) with two *high-spin* Co^{II} atoms and two radical neutral ligands, L3^{\bullet} . The corresponding broken-symmetry states were calculated starting from this *high-spin* complex. The spin-density distributions for all calculated states are visualised in Figure 11, and the relative energies are compiled in Table 5. The relative energies clearly argue for a dominating antiferromagnetic coupling between the Co and adjacent ligand spin centers. The antiferromagnetic coupling between the two metals is much weaker. With the help of the Ising operator and the calculated relative energies of the BS states, the coupling constants J could be estimated.^[64] A coupling constant $J_{\text{L3-Co}}$ of -188 cm^{-1} was obtained for the magnetic coupling between radical ligand and adjacent Co atom. The coupling of the two Co spin centers, $J_{\text{Co-Co'}}$, amounts to only ca. -16 cm^{-1} . As expected, the coupling constant describing coupling between the ligand radical and the remote Co atom, $J_{\text{L3-Co'}}$, is again smaller (-6 cm^{-1}). Finally, the coupling constant between the two radical ligands, $J_{\text{L3-L3'}}$, is ca. $+3 \text{ cm}^{-1}$. The quite large antiferromagnetic coupling between the radical ligand and the adjacent cobalt explains the relatively low room temperature χT value of $3.14 \text{ cm}^3 \text{ K mol}^{-1}$ from SQUID measurements on the solid material and $2.99 \text{ cm}^3 \text{ K mol}^{-1}$ from magnetic measurements with the Evans NMR method in solutions. We

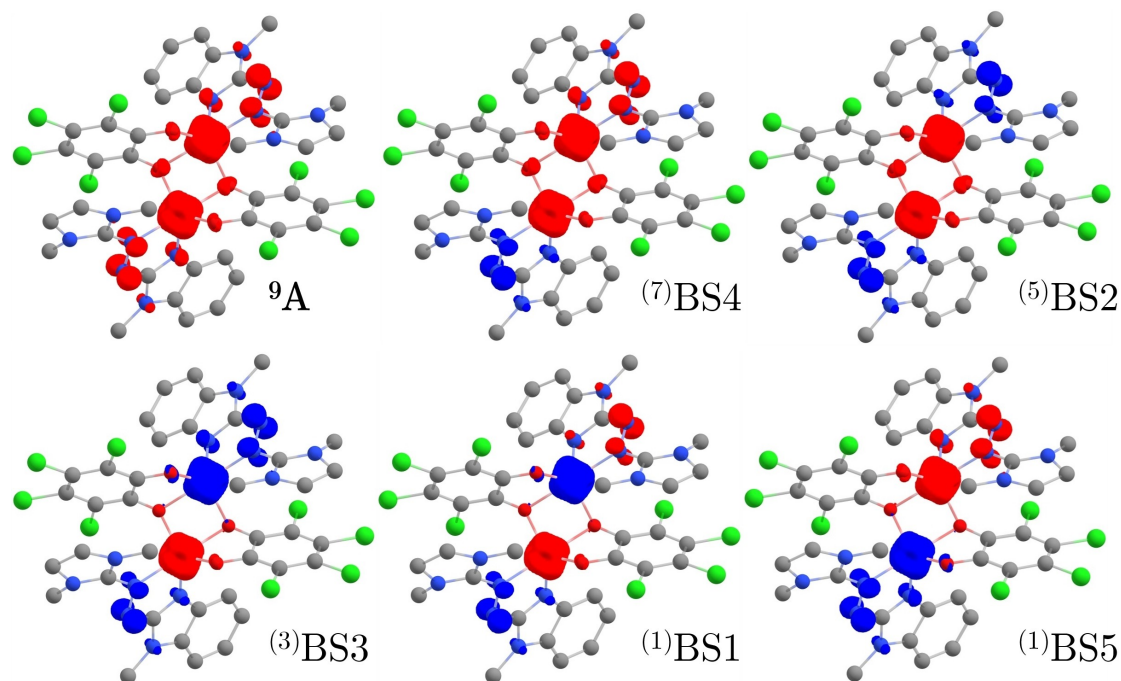
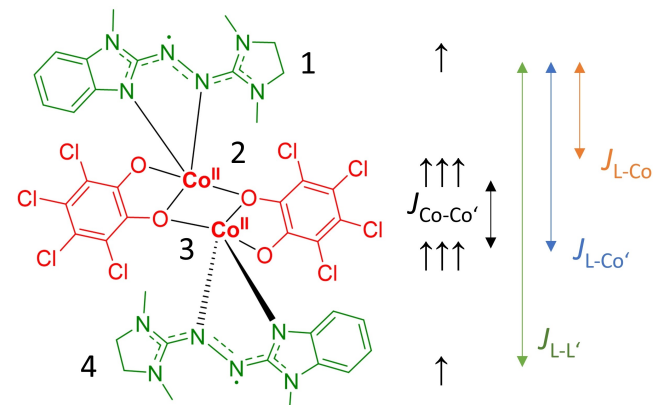


Figure 11. Spin-density distribution from B3LYP + D3/def2-TZVP calculations for the 9A high-spin state of $[\text{Co}_2(\text{Cl}_4\text{-cat})_2(\text{L}_3)_2]$ and the corresponding broken-symmetry states (isovalue 0.02, red and blue denote opposite signs of the spin density).

Table 5. Relative energies (in cm^{-1}) and energies expressed by the J_{ij} parameters as derived from the Ising operator model ($J_{12}=J_{34}=J_{\text{L}_3\text{-Co}}$, $J_{13}=J_{24}=J_{\text{L}_3\text{-Co}'}$, $J_{23}=J_{\text{Co-Co}'}$, $J_{14}=J_{\text{L}_3\text{-L}_3'}$) for the 9A high-spin state and the related broken-symmetry states of the $[\text{Co}_2(\text{Cl}_4\text{-cat})_2(\text{L}_3)_2]$ complex from B3LYP + D3/def2-TZVP calculations.

							$\Delta E / \text{cm}^{-1}$	Energy expressed by the J_{ij} values
	L3	Co	Co'	L3'	S_z	$\langle S^2 \rangle$		
9A	↑	(↑↑↑)	(↑↑↑)	↑	4	20.030	0	$-2(\frac{3}{4}J_{12} + \frac{3}{4}J_{13} + 2\frac{1}{4}J_{23} + \frac{3}{4}J_{24} + \frac{3}{4}J_{34} + \frac{1}{4}J_{14})$
$^{(1)}\text{BS5}$	↑	(↑↑↑)	(↓↓↓)	↓	0	4.017	-175.2	$-2(\frac{3}{4}J_{12} - \frac{3}{4}J_{13} - 2\frac{1}{4}J_{23} - \frac{3}{4}J_{24} + \frac{3}{4}J_{34} - \frac{1}{4}J_{14})$
$^{(7)}\text{BS4}$	↑	(↑↑↑)	(↑↑↑)	↓	3	12.969	-574.3	$-2(\frac{3}{4}J_{12} + \frac{3}{4}J_{13} + 2\frac{1}{4}J_{23} - \frac{3}{4}J_{24} - \frac{3}{4}J_{34} - \frac{1}{4}J_{14})$
$^{(3)}\text{BS3}$	↑	(↑↑↑)	(↓↓↓)	↑	1	4.961	-720.9	$-2(\frac{3}{4}J_{12} - \frac{3}{4}J_{13} - 2\frac{1}{4}J_{23} + \frac{3}{4}J_{24} - \frac{3}{4}J_{34} + \frac{1}{4}J_{14})$
$^{(5)}\text{BS2}$	↓	(↑↑↑)	(↑↑↑)	↓	2	7.907	-1154.5	$-2(-\frac{3}{4}J_{12} - \frac{3}{4}J_{13} + 2\frac{1}{4}J_{23} - \frac{3}{4}J_{24} - \frac{3}{4}J_{34} + \frac{1}{4}J_{14})$
$^{(1)}\text{BS1}$	↑	(↓↓↓)	(↑↑↑)	↓	0	3.902	-1266.9	$-2(-\frac{3}{4}J_{12} + \frac{3}{4}J_{13} - 2\frac{1}{4}J_{23} + \frac{3}{4}J_{24} - \frac{3}{4}J_{34} - \frac{1}{4}J_{14})$

abstained from fitting the magnetometric (SQUID) curve due to the multitude of parameters that have to be considered in such a fit. First, there are four coupling constants ($J_{\text{L}_3\text{-Co}}$, $J_{\text{L}_3\text{-Co}'}$, $J_{\text{Co-Co}'}$, and $J_{\text{L}_3\text{-L}_3'}$). Then, at least three g factors have to be included.

Conclusions

Coordination compounds with redox-active ligands are currently studied intensively because of the additional opportunities in catalysis and materials science that arise from the ligand redox properties.^[1-10] Usually, only one type of redox-active ligand is present in these complexes. Compounds exhibiting

two different types of redox-active ligands are uncommon, despite of the interesting electronic structures and possible reactivity that one could envision from such combinations. Hence, the integration of two types of redox-active ligands allows the design of multiple center redox systems. In this work, the first complexes were reported in which redox-active bisguanidine or urea azine ligands are combined with another type of redox-active ligand (oxolene ligands) in coordination compounds, resulting in four or six center redox systems. A rational synthesis of these complexes is possible due to the complementary charge regimes of the different types of applied redox-active ligands. Electron-transfer processes between the ligands occur; all synthesised complexes exhibit one or two radical ligands.

First, it is shown that reaction between a neutral bisguanidine (L1 or L2) and a cobalt-bis-semiquinonate complex leads, in dependence of the redox potential of the semiquinonato ligands, to a Co^{II} complex with two semiquinonato ligands and a neutral bisguanidine ligand, or to a Co^{III} complex with two catecholato ligands and a radical monocationic bisguanidine ligand.

Then, the reaction between a cobalt bis-semiquinonato complex and a protonated urea azine ligand, HL3, is shown to lead to an unprecedented dinuclear complex with two bridging catecholato ligands and two neutral, radical urea azine ligands, L3*. The results show that the two types of redox-active ligands compete for the electron density, and variations of the redox potential could be used to alter the resulting electronic structures. The intriguing electronic structures, that follow from the combination of two different types of redox-active ligands, could be evaluated by their characteristic magnetic and optical properties. Using the strategy established in this work (with different charge regimes of the two types of redox-active ligands), it should be possible to synthesise a variety of coordination compounds with two types of redox-active ligands. The interplay and competition of these ligands should open up new opportunities in catalysis and materials science.

Experimental Section

The synthetic details and analytical data for all compounds as well as the details of the quantum-chemical (DFT) calculations are included in the Supporting Information.

Deposition Numbers 2176177 ([Co(Cl₄-cat)(L1)], 2176178 ([Co(Cl₄-cat)(L2)], 2176179 ([Co(Cl₄-cat)(L5)], 2176180 ([Co(L3)₂]), 2176181 ([H₂L3]([L3]Co(Cl₄-cat)₂]), and 2176182 ([Co₂(Cl₄-cat)₂(L3)₂]) contain the supplementary crystallographic data for this paper. These data are provided free of charge by the joint Cambridge Crystallographic Data Centre and Fachinformationszentrum Karlsruhe Access Structures service.

Acknowledgements

The authors gratefully acknowledge continuous financial support by the Deutsche Forschungsgemeinschaft (DFG). Quantum chemical calculations were carried out with the aid of

BwForCluster JUSTUS 2 (grant No. INST 40/575-1 FUGG, JUSTUS 2). Open Access funding enabled and organized by Projekt DEAL.

Conflict of Interest

The authors declare no conflict of interest.

Data Availability Statement

The data that support the findings of this study are available in the supplementary material of this article.

Keywords: azine · cobalt · guanidine · radical ligand · redox-active ligand

- [1] W. I. Dzik, J. I. van der Vlugt, J. N. H. Reek, B. de Bruin, *Angew. Chem.* **2011**, *123*, 3416–3418; *Angew. Chem. Int. Ed.* **2011**, *50*, 3356–3358.
- [2] J. I. van der Vlugt, *Eur. J. Inorg. Chem.* **2012**, 363–375.
- [3] D. L. J. Broere, R. Plessius, J. I. van der Vlugt, *Chem. Soc. Rev.* **2015**, *44*, 6886–6915.
- [4] J. Jacquet, M. Desage-El Murr, L. Fensterbank, *ChemCatChem* **2016**, *8*, 3310–3316.
- [5] J. I. van der Vlugt, *Chem. Eur. J.* **2019**, *25*, 2651–2662.
- [6] A. Das, Y. Ren, C. Hessin, M. Desage-El Murr, *Beilstein J. Org. Chem.* **2020**, *16*, 858–870.
- [7] A. Das, C. Hessin, Y. Ren, M. Desage-El Murr, *Chem. Soc. Rev.* **2020**, *49*, 8840–8867.
- [8] N. P. van Leest, F. J. de Zwart, M. Zhou, B. de Bruin, *JACS Au* **2021**, *1*, 1101–1115.
- [9] T. Tezgerevska, K. G. Alley, C. Boskovic, *Coord. Chem. Rev.* **2014**, *268*, 23–40.
- [10] H.-J. Himmel, *Inorg. Chim. Acta* **2018**, *481*, 56–68.
- [11] C. G. Pierpont, *Coord. Chem. Rev.* **2001**, *216–217*, 99–125.
- [12] D. N. Hendrickson, C. G. Pierpont, *Top. Curr. Chem.* **2004**, *234*, 63–95.
- [13] A. Dei, D. Gatteschi, C. Sangregorio, L. Sorace, *Acc. Chem. Res.* **2004**, *37*, 827–835.
- [14] E. Evangelio, D. Ruiz-Molina, *Eur. J. Inorg. Chem.* **2005**, 2957–2971.
- [15] O. Sato, J. Tao, Y.-Z. Zhang, *Angew. Chem.* **2007**, *119*, 2200–2236; *Angew. Chem. Int. Ed.* **2007**, *46*, 2152–2187.
- [16] E. Evangelio, D. Ruiz-Molina, *C. R. Chim.* **2008**, *11*, 1137–1154.
- [17] J. S. Miller, K. S. Min, *Angew. Chem.* **2009**, *121*, 268–278; *Angew. Chem. Int. Ed.* **2009**, *48*, 262–272.
- [18] A. Dei, L. Sorace, *Appl. Magn. Reson.* **2010**, *38*, 139–153.
- [19] T. Tezgerevska, K. G. Alley, C. Boskovic, *Coord. Chem. Rev.* **2014**, *268*, 23–40.
- [20] N. A. Vázquez-Mera, F. Novio, C. Roscini, C. Bellacanzone, M. Guardingo, J. Hernando, D. Ruiz-Molina, *J. Mater. Chem. C* **2016**, *4*, 5879–5889.
- [21] F. Novio, E. Evangelio, N. Vázquez-Mera, P. González-Monje, E. Bellido, S. Mendes, N. Kehagias, D. Ruiz-Molina, *Sci. Rep.* **2012**, *3*:1708, 1–7.
- [22] A. Bencini, A. Caneschi, C. Carbonera, A. Dei, D. Gatteschi, R. Righini, C. Sangregorio, J. Van Slageren, *J. Mol. Struct.* **2003**, *656*, 141–154.
- [23] D. M. Adams, B. Li, J. D. Simon, D. N. Hendrickson, *Angew. Chem.* **1995**, *107*, 1580–1582; *Angew. Chem. Int. Ed.* **1995**, *34*, 1481–1483.
- [24] D. M. Adams, D. N. Hendrickson, *J. Am. Chem. Soc.* **1996**, *118*, 11515–11528.
- [25] P. Gütllich, A. Die, *Angew. Chem.* **1997**, *109*, 2852–2855; *Angew. Chem. Int. Ed.* **1997**, *36*, 2734–2736.
- [26] a) O. Sato, S. Hayami, Z.-z. Gu, K. Takahashi, R. Nakajima, K. Seki, A. Fujishima, *J. Photochem. Photobiol. A* **2002**, *149*, 111–114; b) O. Sato, S. Hayami, Z.-z. Gu, K. Takahashi, R. Nakajima, A. Fujishima, *Chem. Phys. Lett.* **2002**, *355*, 169–174.
- [27] C. Carbonera, A. Die, J.-F. Létard, C. Sangregorio, L. Sorace, *Angew. Chem.* **2004**, *116*, 3197–3200; *Angew. Chem. Int. Ed.* **2004**, *43*, 3136–3138.

- [28] P. Dapporto, A. Die, G. Poneti, L. Sorace, *Chem. Eur. J.* **2008**, *14*, 10915–10918.
- [29] R. D. Schmidt, D. A. Shultz, J. D. Martin, P. D. Boyle, *J. Am. Chem. Soc.* **2010**, *132*, 6261–6273.
- [30] C. Roux, D. M. Adams, J. P. Itié, A. Polian, D. N. Hendrickson, M. Verdaguer, *Inorg. Chem.* **1996**, *35*, 2846–2852.
- [31] S.-Q. Wu, M. Liu, K. Gao, S. Kanegawa, Y. Horie, G. Aoyama, H. Okajima, A. Sakamoto, M. L. Baker, M. S. Huzan, P. Bencok, T. Abe, Y. Shiota, K. Yoshizawa, W. Xu, H.-Z. Kou, O. Sato, *Nat. Commun.* **2020**, *11*, 1992:1–8.
- [32] P. Sadhukhan, S.-Q. Wu, J. I. Lng, T. Nakanishi, S. Kanegawa, K. Gao, K. Yamamoto, H. Okajima, A. Sakamoto, M. L. Baker, T. Kroll, D. Sokaras, A. Okazawa, N. Kojima, Y. Shiota, K. Yoshizawa, O. Sato, *Nat. Commun.* **2021**, *12*, 4836:1–9.
- [33] K. S. Min, A. G. DiPasquale, A. L. Rheingold, H. S. White, J. S. Miller, *J. Am. Chem. Soc.* **2009**, *131*, 6229–6236.
- [34] L. Lohmeyer, F. Schön, E. Kaifer, H.-J. Himmel, *Angew. Chem. Int. Ed.* **2021**, *60*, 10415–10422; *Angew. Chem.* **2021**, *133*, 10506–10514.
- [35] L. Lohmeyer, E. Kaifer, H.-J. Himmel, *Inorg. Chem.* **2022**, *61*, 8440–8454.
- [36] R. Plessius, N. Orth, I. Ivanović-Burmazović, M. A. Siegler, J. N. H. Reek, J. I. van der Vlugt, *Chem. Commun.* **2019**, *55*, 12619–12622.
- [37] P. Singh, A. K. Das, B. Sarkar, M. Niemeyer, F. Roncaroli, J. A. Olabe, J. Fiedler, S. Zláliš, W. Kaim, *Inorg. Chem.* **2008**, *47*, 7106–7113.
- [38] J. Pellegrino, R. Hübner, F. Doctorovich, W. Kaim, *Chem. Eur. J.* **2011**, *17*, 7868–7874.
- [39] A. K. Das, B. Sarkar, C. Duboc, S. Strobel, J. Fiedler, S. Zláliš, G. K. Lahiri, W. Kaim, *Angew. Chem.* **2009**, *121*, 4306–4309; *Angew. Chem. Int. Ed.* **2009**, *48*, 4241–4245.
- [40] A. K. Das, B. Sarkar, J. Fiedler, S. Zláliš, I. Hartenbach, S. Strobel, G. K. Lahiri, W. Kaim, *J. Am. Chem. Soc.* **2009**, *131*, 8895–8902.
- [41] D. M. Adams, A. Die, A. L. Rheingold, D. N. Hendrickson, *J. Am. Chem. Soc.* **1993**, *115*, 8221–8229.
- [42] D. F. Schrempf, E. Kaifer, H. Wadepohl, H.-J. Himmel, *Chem. Eur. J.* **2016**, *22*, 16187–16199.
- [43] D. F. Schrempf, S. Leingang, M. Schnurr, E. Kaifer, H. Wadepohl, H.-J. Himmel, *Chem. Eur. J.* **2017**, *23*, 13607–13611.
- [44] M. Werr, E. Kaifer, M. Enders, A. Asyuda, M. Zharnikov, H.-J. Himmel, *Angew. Chem.* **2021**, *133*, 23641–23652; *Angew. Chem. Int. Ed.* **2021**, *60*, 23451–23462.
- [45] L. Lohmeyer, E. Kaifer, M. Enders, H.-J. Himmel, *Chem. Eur. J.* **2021**, *27*, 11852–11867.
- [46] R. Maskey, C. Bendel, J. Malzacher, L. Greb, *Chem. Eur. J.* **2020**, *26*, 17386–17389.
- [47] M. T. Huynh, C. W. Anson, A. C. Cavell, S. S. Stahl, S. Hammes-Schiffer, *J. Am. Chem. Soc.* **2016**, *138*, 15903–15910.
- [48] M. W. Lehmann, D. H. Evans, *J. Electroanal. Chem.* **2001**, *500*, 12–20.
- [49] M. W. Lehmann, D. H. Evans, *J. Phys. Chem. B* **2001**, *105*, 8877–8884.
- [50] R. M. Buchanan, B. J. Fitzgerald, C. G. Pierpont, *Inorg. Chem.* **1979**, *18*, 3439–3444.
- [51] M. A. Ribeiro, D. E. Stasiw, P. Pattison, P. R. Raithby, D. A. Shultz, C. B. Pinheiro, *Cryst. Growth Des.* **2016**, *16*, 2385–2393.
- [52] L. Leroy, T. M. Francisco, H. J. Shepherd, M. R. Warren, L. K. Saunders, D. A. Shultz, P. R. Raithby, C. B. Pinheiro, *Inorg. Chem.* **2021**, *60*, 8665–8671.
- [53] S. N. Brown, *Inorg. Chem.* **2012**, *51*, 1251–1260.
- [54] D. F. Evans, *J. Chem. Soc.* **1959**, 2003–2005.
- [55] D. H. Grant, *J. Chem. Educ.* **1995**, *72*, 39–40.
- [56] a) G. A. Bain, J. F. Berry *J. Chem. Educ.* **2008**, *85*, 4, 532–536; b) O. Kahn, *Molecular Magnetism*; Wiley-VCH: New York, **1993**.
- [57] H. Herrmann, M. Reinmuth, S. Wiesner, O. Hübner, E. Kaifer, H. Wadepohl, H.-J. Himmel, *Eur. J. Inorg. Chem.* **2015**, 2345–2361.
- [58] S. M. Carter, A. Sia, M. J. Shaw, A. F. Heyduk, *J. Am. Chem. Soc.* **2008**, *130*, 5838–5839.
- [59] C. J. Brown, *Acta Crystallogr.* **1966**, *21*, 170–174.
- [60] A. W. Addison, T. N. Rao, J. Reedijk, J. van Rijn, G. C. Verschoor, *J. Chem. Soc. Dalton Trans.* **1984**, 1349–1356.
- [61] See, for example: D. L. J. Broere, N. P. van Leest, B. de Bruin, M. A. Siegler, J. I. van der Vlugt, *Inorg. Chem.* **2016**, *55*, 8603–8611.
- [62] N. P. van Leest, W. Stroek, M. A. Siegler, J. I. van der Vlugt, B. de Bruin, *Inorg. Chem.* **2020**, *59*, 12903–12912.
- [63] See, for example, the discussion in: N. P. van Leest, M. A. Tepaske, J.-P. H. Oudsen, B. Venderbosch, N. R. Rietdijk, M. A. Siegler, M. Tromp, J. I. van der Vlugt, B. de Bruin, *J. Am. Chem. Soc.* **2020**, *142*, 552–563.
- [64] B. Eberle, M. Damjanovic, M. Enders, S. Leingang, J. Pfisterer, C. Krämer, O. Hübner, E. Kaifer, H.-J. Himmel, *Inorg. Chem.* **2016**, *55*, 1683–1696.

Manuscript received: June 10, 2022

Accepted manuscript online: July 27, 2022

Version of record online: August 31, 2022